Particle Loading Tests on HEPA Flat Sheet Media at Sub-Ambient Pressures Using a Lunar Dust Simulant

Juan H. Agui[1] and Robert D. Green.[2]
NASA Glenn Research Center, Cleveland, OH 44135

Gordon M. Berger[3]
Universities Space Research Association, Cleveland, OH 44135

Matthew E. Johnson[4]
Jacobs Technology Inc., Houston, TX, 77058, USA

and

Gary L. Brown[5]
Barrios Technology LTD, Houston, TX, 77058

When humans return to the moon under the NASA Artemis program, their activities on the lunar surface will inevitably lead to the intrusion of lunar dust into the lander cabin. Subsequently the crew would be exposed to the potential hazards of lunar dust and the possibility of ensuing contaminant transfer into orbiting segments after docking. The spacecraft's cabin filtration system will need to be effective at removing the airborne lunar dust to properly purify the breathable cabin air and minimize the spreading of the dust inside the vehicle and orbital segments over the mission duration. The fine nature of the lunar dust will require high efficiency filtration, such as HEPA. Therefore, a series of tests were performed in a specially designed recirculating sealed flow loop, for testing filter media and filter elements at the NASA Glenn Research Center. The flow loop was used to assess the performance and capacity of flat sheet filter media at representative cabin pressures using JSC-1AF lunar dust simulant and at high rates of particle loading. The pressure drop across the flat sheet filter media sample was measured as a function of dust load at ambient pressure and at two sub-ambient pressures, 0.0703 MPa and 0.0565 MPa. The flow velocity on the front face of the media was scaled relative to its pleated configuration. The challenge particle flows were generated by a custom designed particle generator that introduced dispersed particles of the lunar simulant at high concentrations. An optical particle counting instrument provided filter efficiency measurements within the sealed environment. The pressure drop was found to increase linearly with the amount of dust load on the media, for all test conditions, while the starting pressure drop was found to be lower at the lowest sub-ambient pressure case. High filter efficiency was maintained after high particle loads on the media.

Nomenclature

act	=	actual conditions
acfm	=	actual cubic feet per minute
ASHRAE	=	American Society of Heating, Refrigerating and Air-Conditioning Engineers

---

[1] Aerospace Engineer, Thermal Systems and Transport Processes Branch, 21000 Brookpark Road, MS 77-5.
[2] Aerospace Engineer, Thermal Systems and Transport Processes Branch, 21000 Brookpark Road, MS 86-8.
[3] Research Associate, University Space Research Association, NASA-GRC, 21000 Brookpark Road, MS 110-3, Cleveland, OH 44135.
[4] Matthew E. Johnson, EC3 - Gateway ECLSS, NASA Johnson Space Center, 2101 NASA Pkwy, Houston, TX.
[5] Principal Senior Engineer, Gateway Systems Engineering & Integration, 2101 NASA Pkwy, Houston, TX.

C_c	=	Cunningham slip correction factor
CCD	=	Charged-Coupled Device
BFE	=	Bacterial Filter Elements
DSLR	=	digital single-lens reflex camera
E	=	Filter efficiency
ECLSS	=	Environmental Control and Life Support System
HEPA	=	high efficiency particulate air
HLS	=	Human Landing System
IEST	=	Institute of Environmental Sciences and Technology
ISS	=	International Space Station
NIOSH	=	National Institute for Occupational Safety and Health
P	=	flow rate in cubic feet per minute
PSD	=	particle size distribution
Q	=	flow rate in cubic feet per minute
scfm	=	standard cubic feet per minute
std	=	standard conditions
T	=	temperature
ϕ	=	relative humidity

I. Introduction

When humans return to the moon under the NASA Artemis program, their activities on the lunar surface will inevitably lead to the intrusion of lunar dust into the lander cabin. As in the Apollo program, lunar dust transport occurs when the crew re-enters the cabin from multiple surface sorties where the regolith covers the space suits, tools and equipment. One of the inherent properties of the lunar dust is its ability to coat surfaces, where it eventually gets liberated into the cabin air. To control the airborne particles and remove them, HEPA type filters are proposed, based on the success of terrestrial and ISS applications. If it can be done effectively, the spacecraft's cabin filtration system will remove the airborne lunar dust to properly purify the breathable cabin air and minimize the spread of the dust throughout the vehicle and orbital segments over the mission duration. The very small size particles in the 0.2-10 micron range are the most troublesome for crew health, but also can cause damage to equipment and degrade performance. Although HEPA filtration performance is well understood when subjected to common dust particles, there is very little data on its effectiveness in a lunar dust environment, and therefore testing has been proposed to characterize filter efficiency, surface loading, and pressure drop under simulated cabin pressures expected during lunar missions. This data is critical in driving architectural selections for air revitalization systems on lunar landers, Gateway (NASA's planned lunar orbiting outpost) habitable modules, and even lunar habitats.

II. HEPA filters performance and test methods

HEPA filtration is the gold standard in environments where stringent air quality standards and contamination control must be maintained, such as clean rooms, nuclear facilities, and hospitals. The ISS also uses HEPA filters to control airborne particulates and bacterial aerosols; these are known as Bacterial Filter Elements (BFE). HEPA filters capture particles in the nanometer to millimeter sizes with high capturing efficiency, typically upwards of 99.97%. The three main particle capturing mechanisms that contribute to filter efficiency in media filters- diffusion, interception, and inertial impaction- are responsible for capturing over this wide range of particle sizes. The smallest particles, nanometer to submicron in size, are caught by diffusional deposition onto the fibers due to the local random motion imparted on them by Brownian molecular forces. Slightly larger particles that are able to follow the flow streamlines through the fiber matrix are intercepted by direct contact onto the fibers, and largest and more inertial particles are caught by direct impact onto the fibers. High filter efficiency leads to high particle loading which has implications for both the filter resistance and the collection efficiency.

A. Particle Loading

As particles are collected through the depth of the filter during loading, known as depth filtration, they build up onto the fibers and essentially thicken them. As a result, the pressure drop tends to increase because of the growth and rough morphology of adhered particles on the fibers. After some level of depth loading, the particles start to surface load and consequently build up a dust cake on the front surface of the filter. Along with the increased pressure drop, the filter efficiency will also tend to increase above its baseline clean filter efficiency. The loaded particles on the individual fibers become part of the fiber structure, enhancing the surface area and contact points for additional particle capture and attaining a fractional increase in capturing efficiency. The enhanced particle capture on the fibers tends to favor larger particles over smaller ones, resulting in a size dependency in particle capture on the loaded media.[1] Depending on the level of loading and type of filter media used, the loading phenomenon can bring about significant changes to filter performance. It can result in the onset of accelerated increases of pressure drop, and eventually can lead to clogging of the filter where the pressure drop increases two-fold or more beyond the baseline pressure drop and continued operation is inadvisable due to the added stress and load to the ventilation system or spacecraft ECLSS. Therefore, special consideration must be taken in the design of the HEPA filter system and its operation for deep-space spaceflight. This will ensure the continued nominal performance of the filter system over its lifetime, particularly if it has to handle the intrusion of surface dust during lunar and Martian planetary missions.

The literature reports on the effect of accelerated loading performance of various filter types. Zhao et al.[2] performed salt crystal loading on various filter media to show the effect of media type and filter design, including the use of woven (surface filtering) and non-woven (depth filtering) media, and activated carbon enhanced media. They observed non-linear increases in pressure drop and non-linear decreases in penetration (i.e. increases in efficiency) with mass loading for all the flat sheet media types. The magnitude of these increases varied for the different media types. The non-woven media and media with activated carbon had the smallest increases in pressure drop and attained the larger dust holding capacity (defined as amount of dust captured before exceeding the maximum allowable pressure drop). In tests with pleated panel filters, the media were surface loaded at a lower rate because of the larger total filter surface area and were found to produce linear increases in pressure drop. Hinds and Kadrichu[3] and Novick et al.[4] investigated particle loading on HEPA media and found linear increases in resistance and decreases in penetration up to a media surface load of 2.2 g/cm^2. Novick et al. found that when a dust cake was formed the pressure drop increased with decreases in mass mean particle diameter, indicating that loading with smaller particles leads to more rapid increases in pressure drop through dust cakes.

B. Test Methods

For HEPA filters, the collection efficiency is generally high for particles in the range from 0.05 to 0.5 micron. However, neither the diffusional nor interception mechanisms are very dominant in this particle size range and therefore HEPA filters have a slightly lower efficiency (~ 0.03% reduction in filter efficiency) there. It is in this particle size range where the highest degree of particle penetration occurs and where challenge particles of a specific size, or a narrow size distribution, in this range, called the Most Penetrating Particle Size (MPPS), are used in filter testing.

The key performance characteristics (pressure drop, efficiency) for HEPA filters are rated utilizing an industry set of standards that utilize an oil-based aerosol, either Di(2-Ethylhexyl) Phthalate (or DOP), Di(2-Ethylhexyl) Sebacate (DOS), or Poly-Alpha Olefin (PAO), with a well-characterized particle size distribution. In particular, the Institute of Environmental Sciences and Technology's IEST-RP-CC001.5[4] specification is an overall standard describing the types of HEPA filters along with construction materials and requirements, but also describes the performance requirements (e.g. filter resistance or pressure drop) and need to perform both efficiency and leak test as part of penetration testing. The IEST-RP-CC034.3[5] specification discusses the HEPA leak testing, in particular, the choices of tests, aerosol oils, and recommended test procedures and scan test methods, uniformity of the challenge aerosol, and guide for aerosol particle detector which is dependent on filter type. Finally, ASHRAE 52.2-20[6] is a test method standard for the broader air filter application area, and defines requirements for air velocity and aerosol distribution uniformity of the test measurement system. Alternatively, a solid NaCl generated aerosol, with a similar well-characterized PSD is defined in standards for utilization in certain applications that require testing of filters that are not compatible with oil, for example the NIOSH TEB-APR-STP-0059 procedure used to meet the Code of Federal Regulations (CFR) 42 CFR Part 84, Subpart K, for air-purifying face masks (https://ecfr.io/Title-42/Section-84.174). The current test program adapted elements of the testing protocols from the IEST and ASHRAE standards to perform particle loading tests and determine media resistance and efficiency. However, some variations to these standards were required due to the constraints of sub-ambient operation in the current test configuration.

To address the need for data on the lifetime performance of HEPA filter under conditions encountered during a lunar mission, a series of tests were performed to investigate loading capacity of the filter by characterizing the changes in pressure drop and efficiency with the amount of challenge dust loading. These tests were conducted in GRC's filtration flow loop under simulated cabin pressures and by challenging it with lunar dust simulant.

III. Experimental Setup

The filtration flow loop used at the NASA Glenn Research Center is shown in Fig. 1. Its design and features have been reported in previous publications[6-8] but recent updates in temperature and humidity measurements are presented here. It was designed as a recirculating flow loop fabricated from 6-inch schedule 10 diameter pipe segments, and contains axial fans and a vacuum pump for flow induction and low-pressure operation respectively. An integrated particle dispenser internally introduces challenge particles from within the flow stream. The design of the particle generator can be found in Ref. 9. The dispenser can hold most any type of solid granular particles of uniform or polydisperse size distributions, including lunar and other planetary simulant dust particles. Multiple ports and viewports permit the integration of pressure and velocity sensors, light sources and imagers.

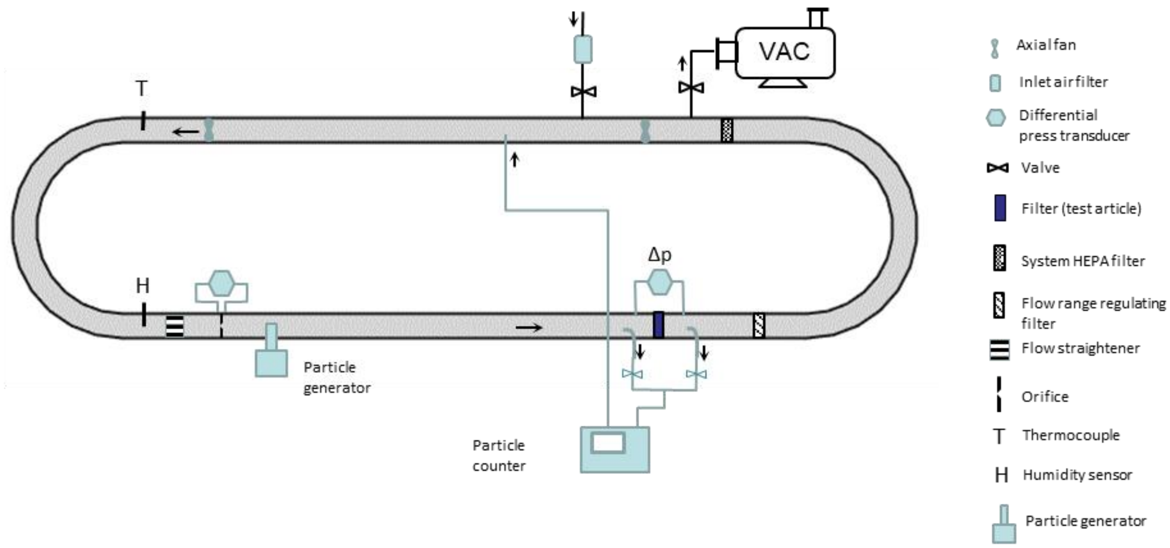

Figure 1: Particle Filtration Flow Loop at the NASA Glenn Research Center (updated schematic, Nov. 2020)

The key components of the facility are shown in the schematic. First, a 300 l/min displacement, scroll oil-free vacuum pump (VAC) was used to achieve the reduced operating pressures required for ECLSS environments in Artemis vehicles, such as the Human Landing System (HLS) and lunar orbiting station (Gateway). DC powered axial fans (main and booster) using variable current and voltage supplies produced the axial flow. A commercial orifice meter consisting of a customized orifice plate and associated differential pressure transducer was utilized for flowrate measurements. Also, a honeycomb-structured flow straightener was used upstream of the orifice meter to break up the vortex that is generated in the 180° elbow. In order to ensure that clean air is returned to the test section of the flow loop, a system HEPA filter was installed in the opposite run of the loop path. The filter test article is installed downstream of the orifice meter, were diagnostic instruments are utilized to characterize performance. In addition, a second system filter was installed further downstream from the test article filter as a means of increasing the flow resistance of the system to achieve the lower flowrate ranges required for the present tests. The particle generator incorporated inside the flow volume does not require any outside delivery source that could compromise the integrity of the enclosed flow. This method overcomes the challenge of incorporating standard filter efficiency test methods, which introduce additional pressurized air and oil-based aerosols. The particle generator internally disperses solid particles and entrains them into the facility flow upstream of the filter test station. The device was filled with either standard calibration particles or planetary simulant dust particles prior to testing.

In addition, a light sheet imaging technique was adapted to qualitatively monitor real-time particle concentrations. The technique is described in Ref. 11. Variations in particle concentrations could be distinguished visually from the real-time image video. Particle concentrations were observed to remain virtually constant over a loading test. However, if an appreciable drop in concentration was noticed, the concentrations were verified with an optical particle counter, described below, and adjustments to the particle generator were performed if concentrations dropped below

10% to 20% of the initial concentration. Quantitatively, the images obtained from this technique can also be analyzed to obtain particle counts and concentrations, and even particle dynamics in a 2-D flow field. This type of data is not covered within the scope of the present paper.

A. Sensors and particle counting

Temperature in the flow loop was measured with a K-type thermocouple ~ 6 diameters upstream of the orifice plate, and humidity was measured with a capacitance-based sensor just ahead of the orifice plate. Humidity sensors of this type have been shown to be minimally influenced by pressure in the range of sub-ambient to ambient pressures used in the current tests.[13] The pressure drop across the filter and the pressure differential across the orifice were also measured by capacitance-based pressure transducers. The orifice meter was calibrated by an independent testing lab capable of testing non-standard geometries (very low beta ratio) and at sub-ambient pressures. The flow coefficients provided by the calibration were used to extract flowrate test data. The calibration data provided a correlation between the pressure transducer voltage (measuring the pressure differential across the orifice plate) and the flow rate standard instrument (in scfm units). The flow velocity data was obtained by converting the standard flowrate to actual units through:

$$Q_{acfm} = Q_{scfm} \frac{P_{std}}{P_{act} - P_{sat}\, \Phi} \left(\frac{T_{act}}{T_{std}}\right)$$

Where Q_{acfm} and Q_{scfm} are the flow rates in units of actual cubic feet per minute (acfm) and standard units (scfm). P_{std}, P_{act}, and P_{sat} are the standard, actual and saturation pressures. T_{act} and T_{std} are the actual (under the actual test conditions) and standard temperatures and φ is the relative humidity. P_{sat} is given by,[14]

$$P_{sat} = \frac{e^{77.3450+.0057T-\frac{7235}{T}}}{T^{8.2}}$$

Where T is the dry bulb temperature of the air. The mean incoming velocity was found by dividing the flowrate, Q_{acfm}, by the filter face area.

The challenge aerosol, consisting of JSC-1AF lunar simulant particles, was introduced into the flow by the particle generator which propelled the particles and dispersed them into the flow. JSC-1AF (described in the next section) is a commonly used lunar simulant and is representative in terms of physical properties of the mare (low-land) regolith on the moon. The holding cavity in the particle generator was capable of holding 3 to 5 grams of lunar simulant in one filling, and could last upwards of 10 hours of testing at a nominal particle generation rate.

A laboratory grade commercial particle counter, a Particle Measurement Systems (PMS) LAS-XII unit, was employed to provide particle count measurements and an estimate of filter efficiency. The LAS-XII is calibrated by the vendor using polystyrene Latex microspheres (PLS). However, the difference in the optical properties of the lunar simulant can result in a variable response from the optical sensor and therefore the actual particle size could differ from that reported by the instrument. To correct for this effect, ancillary tests were conducted using silica microspheres to provide a calibration correction to the measured particle size. Isolating specific size JSC-1AF simulant particles was not practical for this analysis. Simple tests were setup using reference silica particles. JSC-1AF is a mineral based simulant, with SiO_2 being one of the main constituent, ~45% by weight percent (See Ref. 8 for a list of constituents in JSC-1A). For reference, polystyrene spheres which are the particle standards recommended and used by the vendor have a refractive index of 1.6 for particles sizes of 300 nm (see Ref. 15). Commercially available silica spheres, which are closer materially to JSC-1AF, have a refractive index of 1.42. The results of these tests is provided in the associated Table 1 and graphically shown in Fig. 3. This data provided a means of particle size correction that was applied when determining filter efficiency.

Table 1: LAS-XII reported sizes of standard grade silica particles

Silica standard particle size	Particle size reported by the LAS-XII
(μm)	(μm)
0.1	0.118
0.25	0.21
1	0.672
3	1.796

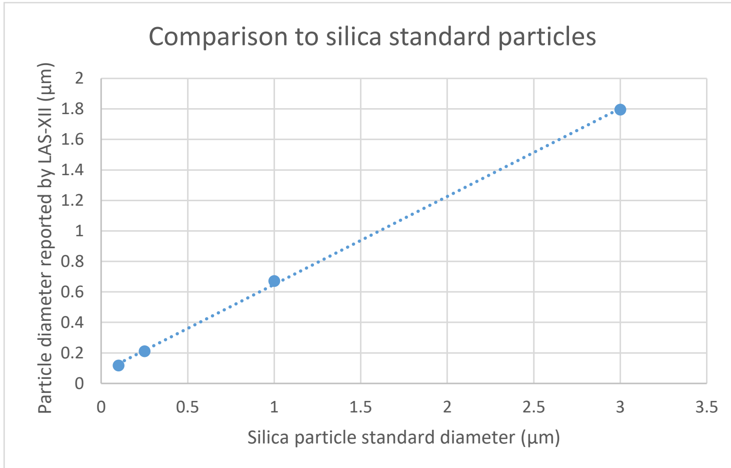

Figure 2: Results for comparison of silica standard particles

In addition, the counting efficiency was also found to be size dependent. Reported drop-offs in counting efficiency using Arizona road dust have been reported for the size range from 0.5 µm to 2 µm with the LAS-XII instrement.[15,16] This is due to differences in Mie-Scattering from particles made of materials with different refractive indices which are accentuated in the size range of 0.5 to 2 µm. Depending on material (Arizona road dust in Ref. 16), larger particles in this size range can have the same scattering signature as smaller particles. For HEPA media, the particle size range of interest for determining efficiency, as described in section II, can range from 0.05 to 0.5 µm, and therefore efficiency calculations using the LAS-XII instrument were assumed to be unaffected by this optical scattering issue.

B. Lunar dust simulant and filter samples

JSC-1AF[17] was selected as the dust simulant, due to its close approximation of expected lunar dust properties, including density, particle size and material makeup. Although the mass-weighted average particle size of JSC-1AF is around 25 microns, the main focus was on collecting particle sizes in the 0.2-10 micron range on the filter media. The simulant was deposited directly into the cavity of the particle generator. The particle generator mixes the lunar simulant sample and then ejects them through a fine mesh screen and into the flow established in the flow loop.

Flat sheet samples of a commercial HEPA grade media were obtained from a filter media manufacturer (Hollingsworth & Vose HB7633 media). The main filter performance specifications of this media is provided in Table 2. Tight quality process control in manufacturing is used to ensure consistency in performance of the media, although there may be slight variations from lot to lot. All tests were conducted with filter media from the same lot. The HEPA flat sheet media was cut to size and a 3D printed ring was glued to the outer perimeter of the media sample to support it and ensure sealing around the edges when the media was installed in the flow loop. The sample was installed between flanges in the test section and sealed within the volume of the flow loop. The differential pressure transducer and optical counter were connected to adjacent ports to measure pressure drop and efficiency. Loading tests were conducted in stages over several days to accumulate enough particle loading mass to assess performance trends and lifetime predictions.

Table 2: HEPA media specifications

Performance parameter	Target value	Units
Basis weight	78	g/m2
Thickness	0.41	mm
Airflow resistance	336	Pa
Penetration	0.015	

After each loading test was completed, the filter sample was uninstalled from the flow loop and weighed with a precision microbalance to measure the amount of accumulated simulant mass on the media sample. A lightweight stand made of metal wire was fashioned to hold the filter sample in place on top of the sensing plate on the microbalance, to avoid any deformation of the media from direct contact with the sensing plate and loss of simulant.

The samples were weighed right after being removed from the flow loop to minimize the moisture from humidity effects, and weighed consecutively three times to reduce mass measurement error. After weighing, the filter samples were flipped vertically, or rotated 180 degrees, to alternate top and bottom orientations of the media during its installation in the flow loop for the next loading stage. This was done to minimize the effects of particle settling on the media, as particles could partially settle towards the bottom of the flow loop and produce a loading gradient on the surface of the media.

IV. Results and Discussion

The flow test conditions were chosen at the relevant operating pressure in the lunar lander cabin (0.0565 MPa) and the Gateway ECLSS cabin which can operate at either 0.0703 MPa or 0.1014 MPa while the other conditions were essentially provided by the laboratory room climate control. Table 3 shows the test conditions. Additionally, the matrix in Table 4 shows all the tests performed and reported herein. Originally, it was intended to have the upper velocity limit to be twice the lower limit value, but operationally it was only feasible to reach about 7 to 7.5 cm/s.

Table 3: Test Conditions

parameter	Value/setting	Units	Comments
Average Filter Face velocity	5.3 , 10.6 (goal)	cm/s	Industry standard flat sheet media velocity, and twice the nominal flow rates
Operating Pressure	0.0565 (8.2) 0.0703 (10.2) 0.1014 (14.7)	MPa (psia)	Represents the ECLSS pressures in the lander and Gateway
Temperature	22-26 (72-79)	ºC (ºF)	Equivalent to the laboratory room temperature
RH	22-40	%	RH was measured but not controlled. Equivalent to the laboratory room RH.
Dust Feed rate	variable	counts/cm^3	Device setting
Sampling rate	10	Hz	Δp, Q, temp, RH

Table 4: Test Matrix

Test #	Pressure kPa (psia)	Face Velocity cm/s	Loading Target mg
TP 1	56.5 (8.2)	5.3	100 – 150
TP 2	70.3 (10.2)	5.3	100 – 150
TP 3	100.3 (14.7)	5.3	100 – 150
TP 4	70.3 (10.2)	7.0	100 – 150

Figure 3 shows the flow resistance, or pressure drop, curves for the HEPA glass media after several particle loading stages for Test Point 1 (TP 1). There are some clear trends in the graphical data. First, at each of the different loading stages the respective pressure drop curve rises quite significantly with face velocity. The pressure drop rises almost in the same proportion as the velocity (i.e. a 50% increase in face velocity produces a ~ 50% increase in pressure drop). Second, each of the curves are shifted upward in pressure drop values with consecutive loading stages, as one might expect when filter media undergoes a loading process. The starting pressure drop was found to vary, at this sub-ambient operating pressure, from the corresponding value specified by the manufacturer (Table 2). For the clean, unused filter (0.0 mg loading), the pressure drop was found around 290 Pa at the nominal test velocity of 5.3 cm/s and air pressure of 0.0565 MPa. Compared to the manufacturer's specification, the pressure drop should be closer to 336 Pa at the industry nominal media velocity and standard atmosphere. Therefore, at .0565 MPa a lower than nominal pressure drop was measured. This can be attributed to increased flow slip effects, at the sub-ambient pressure, over the surface of the media fibers which reduces the drag over the cumulative individual fibers of the filter media. This translates into an operational advantage at reduced pressure.

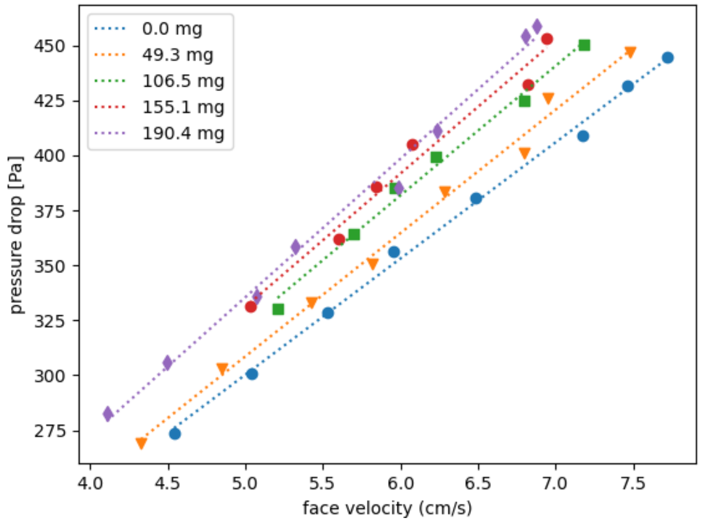

Figure 3: Pressure drop curves after several incremental loading points for HEPA glass media, loading @ 0.0565 MPa with JSC-1AF lunar simulant

Figure 4 shows the loading curve for three different face velocity cases at 0.0565 MPa (8.2 psi). The curves were obtained by interpolating for velocity from the plots in Fig. 4. Even though the pressure drop at the three specific velocities could have been directly measured, it would have taken some time to narrow in on this velocity because of lack of volumetric flow control. The measured value at a specific velocity will also contain some experimental tolerance. Therefore interpolating the values from the resistance curves, and because of the highly linear nature of the curves, was a quicker and cleaner method of obtaining the values at each velocity case. The data reveals that the loading curves increased almost linearly with face velocity for this range of mass loading. The small bump around the surface density of 0.55 mg/cm^2 can be attributed to a small amount of added moisture content from humidity exposure during the weighing process. This was minimized, as discussed in III.B., but some amount of moisture absorption is unavoidable particularly on more humid days, even in the laboratory. The linear trend in mass loading is consistent with published data on solid aerosol mass loading on HEPA media (presented in section II) over the range of media surface loading achieved in the current tests.

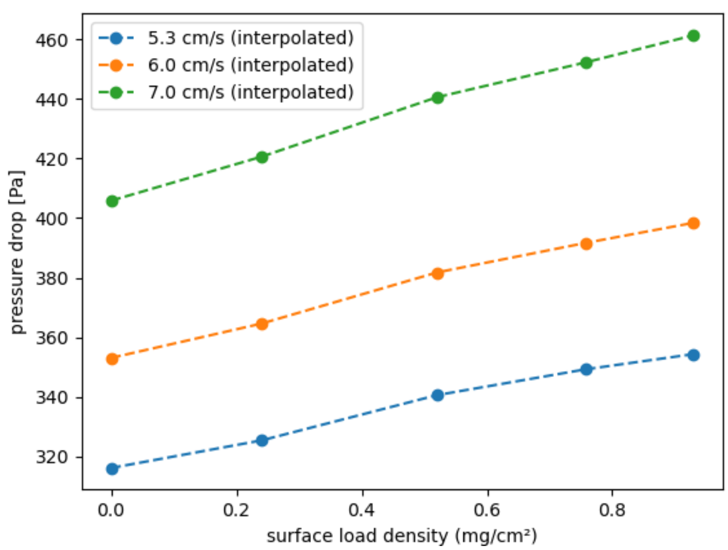

Figure 4: Iso-velocity loading curves for HEPA glass media, loading @ 0.0565 MPa with JSC-1AF lunar simulant.

Figure 5 shows a compilation of loading curves for the four test cases in the test matrix per Table 3. It shows both pressure and velocity effects. As indicated above the starting pressure drop for TP 1 at 0.0565 MPa, was lower than that found at TP2 and TP 3 at 0.0703 MPa and at atmospheric pressure respectively. Also, the starting pressure drop at 0.0703 MPa was virtually the same as in the atmospheric pressure case. Slip flow over the small diameter of the filter fibers and the reduced pressure condition is likely responsible for the reduced pressure drop at this test point. A version of the Cunningham slip correction factor, C_C, provided in terms of particle diameter, d, and pressure, P, is given by[18]:

$$C_C = 1 + \frac{\left[15.6 + 7.0e^{(-.059Pd)}\right]}{Pd}$$

The slip factor is applied to the drag equation resulting in an inverse relation between drag force and the slip factor.

If applied to a fiber of 1 µm diameter at atmospheric pressure, the slip correction factor gives a value of 1.15. The same size fiber at 70.3 kPa has a factor of 1.22 and at 0.0565 MPa has a correction factor of 1.27. These values correspond to increases in slip correction factor of 6% and 11% respectively over the factor at atmospheric conditions. The change in starting pressure drop from TP 3 (atmospheric) and TP 1 (0.0565 MPa) is 8.4%. This is a slightly smaller change than the difference in slip correction factor between these two pressures for a fiber of 1 µm. An average fiber diameter closer to 1.2 µm provides an even better agreement. These simple estimates are relevant since typical filter fiber diameters can span the size range from microns to nanometers. It is not clear why virtually no difference in pressure drop was found between TP 2 and TP3 and further investigation is needed.

When loaded at 7 cm/s (TP4) the resistance curve increased substantially. The increase in drag is in accord with Darcy's Law which dictates that pressure scales linearly with velocity. Specifically, with an increase of 28% in velocity, the starting pressure drop increased by just a slightly larger value of 32%. In a comparison of all four test points, it can be seen that the rise, or slope, in the mass loading curves were similar and thus the filter's loading resistance was found to be independent of test condition.

The mass loading curves in Fig. 5 can be useful in predicting lifetimes of filters. For high efficiency filters, mass surface loading capacity around 2 mg/cm^2 for non-lunar dust have been reported.[2] Also, the ISS program has specified that their filter elements' (BFE's) end of life is reached when accumulating 32g of particulate matter.[19] This would amount to a surface loading of approximately 0.62 mg/cm^2 based on estimate of the total filter surface area of the BFE, which is a more conservative but likely more relevant value for future spaceflight. If the average rate of mass loading is known, or modeled, then the lifetime (in hours) can be predicted assuming this basis is true for lunar dust as well. While this calculation is somewhat idealized, not accounting for general filter construction, particularly the filter pleat design, and the variability in the mass load, it can give a reasonable prediction of filter lifetime. Specifically, difference in pleat design (how tightly packed and pleat depth), the frame construction, and bonding craftsmanship can lead to additional variations in performance.

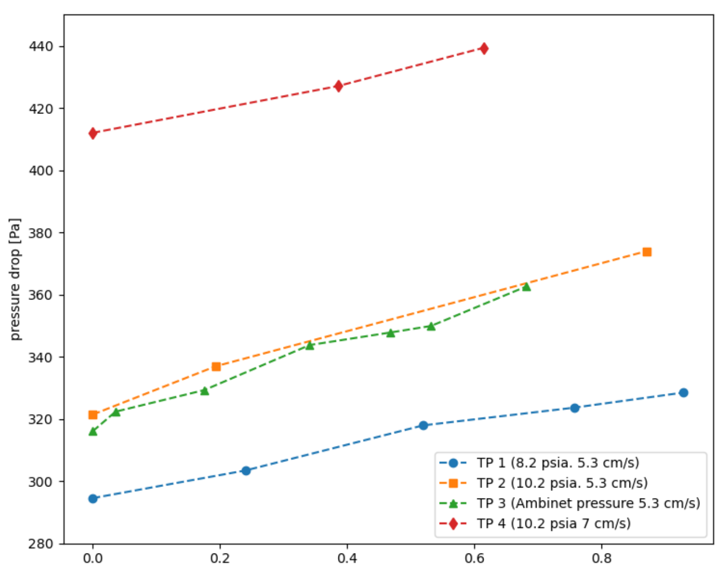

Figure 5: Mass loading curves for TP's 1-4.

In addition to monitoring particle exposure rates during loading experiments, the particle count data below 0.5 μm was used to determine an estimate of filter efficiency and changes in efficiency. The counts were measured one pipe diameter upstream and downstream of the filter test article. The penetration, ***p***, of particles was calculated as the ratio of particle counts upstream to particle counts downstream of the filter. The percent filter efficiency was calculated as,

$$E = (1 - p) * 100$$

Figure 6 shows the measured efficiency after final loading at 0.0565 MPa for the two velocity loading cases. Both plots show the MPPS, based on number counts, around 150 nm, with minimum efficiencies around 99.6% and 98.8% for the 5.3 cm/s and 7 cm/s cases respectively. However, the efficiencies at 0.3 μm, where most HEPA filters are specified, were 99.95% and 99.88% for the 5.3 cm/s and 7 cm/s cases respectively. This finding tracks very well with the HEPA efficiency specification of 99.97% at 0.3 μm within experimental tolerance. The effect of velocity is seen in the clear reduction in efficiency with increased face velocity of 7 cm/s. With increased face velocity there is a loss of diffusional particle capture in the filter media that results in increased penetration of small particles. It should be noted in this analysis that the maximum particle counts during the tests were in the 1000 to 2000 count range. These levels of particle counts were not sufficient to resolve efficiencies to better than ~ 0.05% resolution for a minimum of one particle measured downstream of the filter. A consecutive second count measurement could be used to double the resolution to at best 0.025% resolution. Therefore, the reported efficiencies have error bounds of 0.1% to 0.025% depending on the counts measured at each particle size.

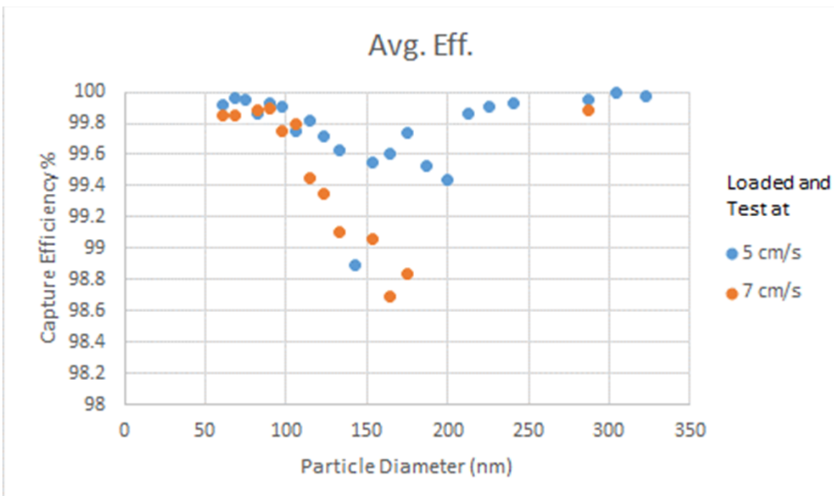

Figure 6: Filter efficiency curves after final loading

The last analysis presented is based on imaging of the loaded filter media surface, as shown in Figure 7. The uniformity of the surface loading was assessed by standard and macro digital single-lens reflex camera (DSLR) 60 mm camera lenses and optical microscopy using a CCD-based machine vision camera. JSC-1AF has a distinctly grey color which facilitated a visual assessment of particle mass loading on the filter samples. All images show fairly uniform loading over the surface of the filter. As described previously, to further ensure uniform loading over the span of the loading sequence, the samples were inverted vertically from its previous orientation when installed back in the flow loop for the next loading stage. Even after their respective first loading test, visual inspection of each of the samples showed that particle loading appeared to be fairly uniform across the surface of the media, indicating minimal particle settling or flow induced separation along the particle flow path. The images clearly show the distinct contrast in shading after different loading conditions, under the same lighting conditions. The loading at 0.55 mg/cm^2 is clearly much lighter in shading than the image at 0.804 mg/cm^2 and 0.988 mg/cm^2. This could be indicative of a transition from depth loading through the interior of the fibrous media and surface loading where the particles are collected on the top surface of the filter. This transition might have taken place sometime during loading between the 0.55 mg/cm^2 and 0.804 mg/cm^2 loading states. Lastly, Fig. 8 shows optical microscopic images at 10X magnification comparing a clean media to one that has been loaded. It shows significant particle build up, obscuring the media fibers, and fairly uniform coverage after loading over the small representative surface area of the media.

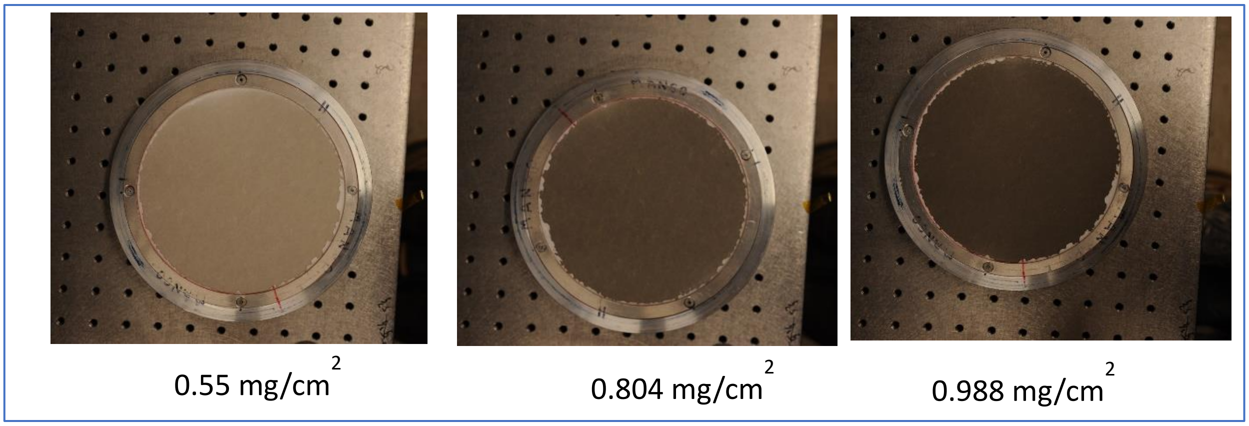

Figure 7: Images of the media after sequential loading stages taken with a 12.1 megapixel DSLR camera.

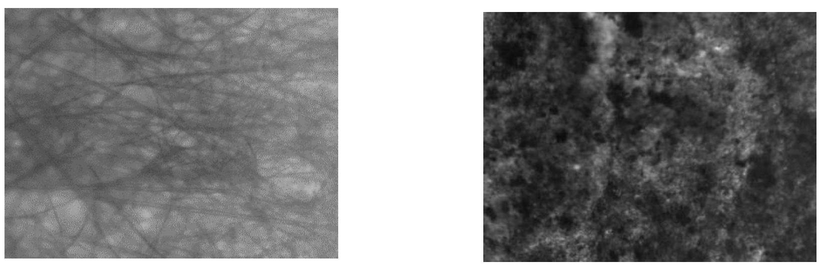

(a) (b)

Figure 8: Microscopic images of a clean (a) and loaded (b) filter media (10X magnification).

V. Conclusions

A series of filter performance and loading tests were conducted on HEPA filter media using JSC-1AF lunar simulant. The test were conducted in NASA Glenn Research Center's filtration flow loop under sub-ambient to ambient pressures that simulate the lunar lander and Gateway cabin operating pressures. The results show that the loading process was reasonably uniform on the filter surface. The pressure drop data increased linearly with dust loading. The data showed that there were pressure and face velocity effects. The starting pressure drop was lower in the 0.0565 MPa case than the 0.0703 MPa and ambient pressure cases. The starting pressure drop and rate of pressure drop increase was higher, in the 0.0703 MPa case, when the face velocity was increased from 5.3 cm/s to 7 cm/s for loading and testing. Finally, the efficiency after loading was found to meet HEPA specification within experimental tolerance, while lower efficiencies were found when the face velocity was increased to 7 cm/s. The results from these HEPA glass media tests will be compared to and supplemented by additional ongoing tests on HLS and Gateway contractor provided high-efficiency filter media, presented in an accompanying paper. This data will also potentially be used to inform future ECLSS HEPA filter designs in the Artemis program.

Acknowledgments

We thank NASA GRC Senior management and the associated Return to Onsite Work (RTOW) Executive Committee for approving laboratory access during the 2020 COVID-19 pandemic to perform the current testing. We would also like to thank Donna Kasper at Hollingsworth & Vose for providing the filter media samples used in completing his work, which was greatly appreciated. Finally, we would like to thank Dr. R. Vijakumar at Airfil LLC for consultation on testing methodology. Trade names and trademarks are used in this report for identification only. Their usage does not constitute an official endorsement, either expressed or implied, by the National Aeronautics and Space Administration.

References

[1]Brown, R.C. Air Filtration, Pargamon Press,1993, Ch. 8.

[2]Zhao, P., Cheng, P. and Tatarchuk, B.J., 2016. Loading of fibrous filter media and newly designed filter configurations by salt particles: An experimental study. AIChE Journal, 62(10), pp.3739-3750.

[3]Hinds, W.C. and Kadrichu, N.P., 1997. The effect of dust loading on penetration and resistance of glass fiber filters. *Aerosol science and technology*, *27*(2), pp.162-173.

[4]Novick, V.J., Monson, P.R. and Ellison, P.E., 1992. The effect of solid particle mass loading on the pressure drop of HEPA filters. Journal of aerosol science, 23(6), pp.657-665.

[5]IEST-RP-CC001.5, "HEPA and ULPA Filters", Institute of Environmental Sciences and Technology, Arlington Heights, IL, 2009

[6]IEST-RP-CC034.3, "HEPA and ULPA Filter Leak Tests", Institute of Environmental Sciences and Technology, Arlington Heights, IL, 2009.

[7]ASHRAE Standard 52.2-20, "Method of Testing General Ventilation Air-Cleaning Devices for Removal Efficiency by Particle Size", American Society of Heating, Refrigerating and Air-Conditioning Engineers, Atlanta, GA, 201.

[8]TEB-APR-STP-0059, NIOSH, "DETERMINATION OF PARTICULATE FILTER EFFICIENCY LEVEL FOR N95 SERIES FILTERS AGAINST SOLID PARTICULATES FOR NON-POWERED, AIR-PURIFYING RESPIRATORS STANDARD TESTING PROCEDURE (STP)", National Institute for Occupational Safety and Health, Dec. 2019

[9]Agui, J.H., 2008. Flow and Particulate Transport Modeling of a Lunar Dust Filtration Testing Facility (No. 2008-01-1961). SAE Technical Paper.

[10]Agui, J.H. and Mackey, J.R., 2009. Development and Testing of a New NASA Lunar Dust Filtration Testing Facility (No. 2009-01-2358). SAE Technical Paper.

[11]Agui, J.H., 2016, April. Filter media tests under simulated Martian atmospheric conditions. In Proceedings of the 15th Biennial ASCE Conference on Engineering, Science, Construction, and Operations in Challenging Environments (pp. 11-15).

[12]Agui, Juan H., and Vijayakumar, R., "System and apparatus for filtering particles". United States. https://www.osti.gov/servlets/purl/1650950, Patent No. 10663376, Issue date 2020-05-26.

[13]Luijten, C.C.M., Van Dongen, M.E.H. and Stormbom, L.E., 1998. Pressure influence in capacitive humidity measurement. Sensors and Actuators B: Chemical, 49(3), pp.279-282.

[14]Engineering ToolBox, (2004). Water Vapor and Saturation Pressure in Humid Air. [online] Available at: https://www.engineeringtoolbox.com/water-vapor-saturation-pressure-air-d_689.html

[15]C.S. Ray, S.T. Reis, S. Sen, J.S. O'Dell, JSC-1A lunar soil simulant: Characterization, glass formation, and selected glass properties, Journal of Non-Crystalline Solids, Volume 356, Issues 44–49, 2010

[16]"Comparison of the TSI Laser Aerosol Spectrometer with the APS and SMPS for Measurement of Particle Size" AAAR (American Association for Aerosol Research) 2009, Poster presentation.

[17]"CHARACTERIZATION SUMMARY OF JSC-1AF LUNAR MARE REGOLITH SIMULANT," https://www.nasa.gov/sites/default/files/atoms/files/jsc-1af_characterization.pdf

[18]Hinds, William C. 1999. Aerosol technology: properties, behavior, and measurement of airborne particles. New York: Wiley.

[19]Perry, J.L., 2005. International Space Station bacteria filter element service life evaluation. NASA TM, 213846, p.2005.